A Nanostructured SiAl0.2O Anode Material for Lithium Batteries

ARTICLE *in* CHEMISTRY OF MATERIALS · SEPTEMBER 2010

Impact Factor: 8.35

1 AUTHOR:

Goojin Jeong
Korea Electronics Technology Institute
53 PUBLICATIONS **1,194** CITATIONS

SEE PROFILE

5570 *Chem. Mater.* **2010,** *22,* 5570–5579
DOI:10.1021/cm101747w

CHEMISTRY OF MATERIALS
Article

A Nanostructured $SiAl_{0.2}O$ Anode Material for Lithium Batteries

Goojin Jeong

Green Energy System Center, Kumoh National Institute of Technology Gumi, Kyeongsangbuk-do, 730-701, Republic of Korea

Young-Ugk Kim*

Battery Development Team, Samsung SDI Co., LTD. Cheonan, Chungcheongnam-do, 330-300, Republic of Korea

Sergey A. Krachkovskiy

Corporate R&D Center, Samsung SDI Co., LTD. Yongin, Gyeonggi-do, 446-577, Republic of Korea

Churl Kyoung Lee

School of Advanced Materials and System Engineering, Kumoh National Institute of Technology Gumi, Kyeongsangbuk-do, 730-701, Republic of Korea

Received June 22, 2010. Revised Manuscript Received August 19, 2010

Silicon monoxide (SiO) is a promising candidate for anodes in lithium rechargeable batteries, because of its large capacity. The initial irreversible reaction and still dissatisfactory capacity retention during cycling, however, hinder its practical application. A nanostructured $SiAl_{0.2}O$ composite material has been developed via mechanochemical synthesis and investigated as an alternative anode. The $SiAl_{0.2}O$ is composed of quantitatively increased silicon nanocrystallites, each of which is less than 10 nm in size, embedded in an amorphous matrix; the compositional structure of the matrix is aluminosilica in which most of Si atoms are neighbored with two Al atoms over oxygen, as confirmed with X-ray diffraction (XRD), solid-state ^{29}Si and ^{27}Al nuclear magnetic resonance (NMR), and transmission electron microscopy (TEM). This electrode exhibits enhanced initial Coulombic efficiency of which the relative increase is $>10\%$, compared to SiO, and also demonstrates improved cycling performance, offering a capacity of 800 mAh/g over 100 cycles. These improvements are attributed to the electrochemically inactive alumina component, which not only replaces part of the SiO_2 phase that is regarded as an origin of initial irreversible reaction but also provides mechanically reinforcing properties, resulting in little pulverization of particles and less change in the impedance of the $SiAl_{0.2}O$ electrode during cycling.

Introduction

Lithium batteries based on graphite as an anode material have been commercially used in portable devices such as cellular phones and laptop computers for about the last two decades. However, as these devices become more multifunctional and compact, a higher energy density of lithium batteries has been in strong demand.[1−4] Even though considerable increases in the energy density of lithium batteries based on the graphite anode materials has been achieved through cell design engineering, the limit has been reached and, finally, the development of advanced electrode materials becomes indispensable to fulfill the demand for increase of energy density. Silicon- or tin-based materials have been considered as alternative anode materials for the higher energy density and they have almost doubled the capacity of graphite.[5,6] Nevertheless, the commercialization of these high-capacity anode materials has been hindered because of capacity fading and dimensional change during charge and discharge cycling, which is widely believed to be caused by a large volumetric change of active materials. In the case of silicon, the volume change can be up to 400% between the delithiated and fully lithiated states, and generated internal stress is accumulated during repetition of this dimensional change.[7] This leads to cracking and fracturing of

*Author to whom correspondence should be addressed. Tel.: +82 54 478 7891. Fax: +82 54 478 7934. E-mail: kyuang@snu.ac.kr.

(1) Bruce, P. G.; Scrosati, B.; Tarascon, J.-M. *Angew. Chem., Int. Ed.* **2008**, *47*, 2930.
(2) Kim, M. G.; Cho, J. *Adv. Funct. Mater.* **2009**, *19*, 1497.
(3) Scrosati, B.; Garche, J. *J. Power Sources* **2010**, *195*, 2419.
(4) Armand, M.; Tarascon, J.-M. *Nature* **2008**, *451*, 652.
(5) Huggins, R. A. In *Advanced Batteries: Materials Science Aspects*; Springer: New York, 2009; Chapter 7.
(6) Yu, Y.; Gu, L.; Wang, C.; Dhanabalan, A.; van Aken, P. A.; Maier, J. *Angew. Chem., Int. Ed.* **2009**, *48*, 6485.
(7) Obrovac, M. N.; Christensen, L.; Le, D. B.; Dahn, J. R. *J. Electrochem. Soc.* **2007**, *154*, A849.

Published on Web 09/03/2010

the active materials, loosening of the electrical network in the electrodes, and, hence, the deterioration of the anodes. Recently, many attempts have been made to overcome these problems. Active/inactive nanostructured materials,[8,9] intermetallic compounds showing topotactic reaction,[10,11] and nanosized arrays or powders such as silicon nanowires[12−14] have been major development approaches, with respect to active materials.

Among the various nanostructured materials, silicon monoxide (SiO) has been attractive as one of promising anode materials, because of its relatively long cycling performance and high gravimetric capacity.[15−20] Unfortunately, there is a fatal drawback in the SiO, that is to say, low initial Coulombic efficiency (ICE), so that the energy density in a full cell system is still not satisfactory. Several studies on the initial irreversible reaction of SiO have been carried out recently. According to the literature,[15−17,21] it can be generally thought that the initial irreversible reaction of SiO is intimately associated with electrochemical reactivity of silicon oxide phases ($Si_2^{(+1)}O$, $Si^{(+2)}O$, $Si_2^{(+3)}O_3$, and $Si^{(+4)}O_2$) in the disproportionated SiO with lithium. SiO is not a homogeneous single-phase compound but is considered to be a nanometer-scale mixture of nanocrystalline silicon and amorphous SiO_2 or other suboxides.[22−24] Bulky silicon dioxide (SiO_2) is normally known as an insulator and does not react electrochemically with lithium. As the domain size of SiO_2, however, approaches the nanoscale and amorphous state, the electrochemical reactivity with lithium appears and exhibits possibilities for use as electrode or electrolyte materials in lithium battery systems.[25,26] As for irreversible reaction products, Yamada at the Hitachi Maxell company[27] presented the Li_4SiO_4 phase, based on the X-ray absorption near-edge structure (XANES) results, and Morita et al.[15] also mentioned lithium silicates such as Li_2SiO_3 and Li_4SiO_4, based on the ex situ XRD and TEM analyses. Miyachi et al.[17,21] reported Li_2O and several lithium silicate phases using X-ray photoelectron spectroscopy (XPS) and TEM analyses, and Guo et al.[28] and Kim et al.[16] also indentified the irreversible phases after the first cycle as Li_2O and Li_4SiO_4, using solid-state ^{7}Li NMR, ^{29}Si NMR, and TEM analysis. However, the reaction mechanism of SiO is still not clear and is controversial, such that more-definitive identifications are necessary. To overcome the problem of the low ICE, many works have been reported, and they were mostly focused on the prelithiation through chemical reaction with lithium. The Li predoping into SiO by lithium metal evaporation,[17] chemical lithiation in certain solutions,[29] and mechanochemical reaction with Li metal[20,30] using a high-energy mechanical milling process were reported. Solid-state reaction via heat treatment with LiOH[18] was also a related report for improvement of the initial charge and discharge behavior. The lithium-inactive metals, such as iron-, nickel-, and titanium-doped SiO thin films were also investigated to increase the ICE by improving the reaction kinetics.[17] However, these treatments are not easy to apply to powder-type materials and have low processability for production. Also, their products are still chemically unstable with regard to handling and must be improved for more-satisfactory cell performances.

In the present work, we have proposed an advanced SiO-based nanostructure material to increase the ICE and improve the cycling performance as well. The first point in approach is to rebuild the matrix phases in SiO. The SiO_2 in disproportionated SiO has been considered as a main matrix phase and a cause of the initial irreversible reaction as previously mentioned. If we could reform the matrix phases to retain less irreversible electrochemical reactivity and more reinforcing mechanical properties, the increased ICE and the improved cycling performance could be expected. The second point is to maintain the island-typed nanostructure of silicon phases embedded in a matrix similar to the SiO. The silicon nanophases in SiO are the main active sites for reversible charge and discharge reactions during cycling, so that the size and crystallinity of the silicon phases are very important factors for overall cell performance, which have been well-established in silicon-based anode materials systems.[1,2] Under these considerations, we tried to partially convert the SiO_2 phases in SiO into other lithium-inactive and mechanically reinforcing metal oxides by chemical reduction of SiO_2 with some elemental metals that are thermodynamically

(8) Yoon, S.; Manthiram, A. *Chem. Mater.* **2009**, *21*, 3898.
(9) Mao, O.; Dahn, J. R. *J. Electrochem. Soc.* **1999**, *146*, 423.
(10) Thackeray, M. M.; Vaughey, J. T.; Johnson, C. S.; Kropf, A. J.; Benedek, R.; Fransson, L. M. L.; Edstrom, K. *J. Power Sources* **2003**, *113*, 124.
(11) Thackeray, M. M.; Vaughey, J. T.; Kahaian, A. J.; Kepler, K. D.; Benedek, R. *Electrochem. Commun.* **1999**, *1*, 111.
(12) Song, T.; Xia, J.; Lee, J.-H.; Lee, D. H.; Kwon, M.-S.; Choi, J.-M.; Wu, J.; Doo, S. K.; Chang, H.; Park, W. I.; Zang, D. S.; Kim, H.; Huang, Y.; Hwang, K.-C.; Rogers, J. A.; Paik, U. *Nano Lett.* **2010**, *10*, 1710.
(13) Chan, C. K.; Peng, H.; Liu, G.; McIlwrath, K.; Zhang, X. F.; Huggins, R. A.; Cui, Y. *Nature Nanotechnol.* **2008**, *3*, 31.
(14) Park, M.-H.; Kim, M. G.; Joo, J.; Kim, K.; Kim, J.; Ahn, S.; Cui, Y.; Cho, J. *Nano Lett.* **2009**, *9*, 3844.
(15) Morita, T.; Takami, N. *J. Electrochem. Soc.* **2006**, *153*, A425.
(16) Kim, T.; Park, S.; Oh, S. M. *J. Electrochem. Soc.* **2007**, *154*, A1112.
(17) Miyachi, M.; Yamamoto, H.; Kawai, H. *J. Electrochem. Soc.* **2007**, *154*, A376.
(18) Veluchamy, A.; Doh, C.-H; Kim, D.-H.; Lee, J.-H.; Lee, D.-J.; Ha, K.-H.; Shin, H.-M; Jin, B.-S.; Kim, H.-S.; Moon, S.-I.; Park, C.-W. *J. Power Sources* **2009**, *188*, 574.
(19) Kim, J.-H.; Sohn, H.-J.; Kim, H.; Jeong, G.; Choi, W. *J. Power Sources* **2007**, *170*, 456.
(20) Yang, X.; Wen, Z.; Xu, X.; Lin, B.; Huang, S. *J. Power Sources* **2007**, *164*, 880.
(21) Miyachi, M.; Yamamoto, H.; Kawai, H.; Ohta, T.; Shirakata, M. *J. Electrochem. Soc.* **2005**, *152*, A2089.
(22) Hohl, A.; Wieder, T.; van Aken, P. A.; Weirich, T. E.; Denninger, G.; Vidal, M.; Oswald, S.; Deneke, C.; Mayer, J.; Fuess, H. *J. Non-Cryst. Solids* **2003**, *320*, 255.
(23) Schulmeister, K.; Mader, W. *J. Non-Cryst. Solids* **2003**, *320*, 143.
(24) Khavryuchenko, O. V.; Khavryuchenko, V. D.; Roszinski, J. O.; Brusilovets, A. I.; Friede, B.; Lisnyak, V. V. *Thin Solid Films* **2006**, *515*, 1280.
(25) Sun, Q.; Zhang, B.; Fu, Z.-W. *Appl. Surf. Sci.* **2008**, *254*, 3780.
(26) Ariel, N.; Ceder, G.; Sadoway, D. R.; Fitzgerald, E. A. *J. Appl. Phys.* **2005**, *98*, 023516.
(27) Yamada, M. Presented at *The 17th Battery Technology Symposium*, Chiba, Japan, 2009; Paper No. No. J2-2.
(28) Guo, B.; Shu, J.; Wanga, Z.; Yang, H.; Shi, L.; Liu, Y.; Chen, L. *Electrochem. Commun.* **2008**, *10*, 1876.
(29) Tabuchi, T.; Yasuda, H.; Yamachi, M. *J. Power Sources* **2005**, *146*, 507.
(30) Liu, Y.; Wen, Z. Y.; Wang, X. Y.; Yang, X. L.; Hirano, A.; Imanishi, N.; Takeda, Y. *J. Power Sources* **2009**, *189*, 480.

feasible for this reaction. According to the Ellingham diagram,[31] aluminum, calcium, magnesium, and lithium can react with SiO_2 and produce both lithium-inactive oxides as other matrix components and additional new silicon phases that are able to participate in reversible reaction with lithium. The Gibbs free energies at room temperature of examples are as follows:

$$3SiO_2 + 4Al = 3Si + 2Al_2O_3 \qquad \Delta G^\circ = -47.42 \text{ kcal/mol} \quad (1)$$

$$SiO_2 + 4Li = Si + 2Li_2O \qquad \Delta G^\circ = -63.54 \text{ kcal/mol} \quad (2)$$

$$SiO_2 + 2Ca = Si + 2CaO \qquad \Delta G^\circ = -83.69 \text{ kcal/mol} \quad (3)$$

$$SiO_2 + 2Mg = Si + 2MgO \qquad \Delta G^\circ = -67.46 \text{ kcal/mol} \quad (4)$$

Of the above candidates, aluminum was selected as a reducing element, because we expected that aluminum oxide as a reaction product is electrochemically inactive and known as an engineering ceramic material that has durable mechanical properties,[32,33] which could offer high resistance against the cracking and fracture that occurs because of the volumetric change of SiO during cycling. To synthesize the nanostructured $SiAl_xO$ materials that satisfy the aforementioned material concepts, we employed a high-energy mechanical milling (HEMM) process, since it is a simple and easily available method in powder metallurgy to prepare nanostructured or amorphous materials and can also carry out chemical reactions among reactants at the same time.[30,34,35] In this study, we focused on a $SiAl_{0.2}O$ material as an anode for lithium batteries and presented its structural, chemical, and electrochemical characteristics with discussions.

Experimental Section

Synthesis of $SiAl_{0.2}O$ Nanocomposite. The nanostructured $SiAl_{0.2}O$ material was prepared using the following synthetic process: SiO powder (>99%, D_{50} = 4 μm, received from Samsung SDI Co., Ltd.) and aluminum metal powder (>99%, D_{50} = 4 μm, purchased from Kojundo Chemical Laboratory Co., Ltd.) were chosen as starting materials for mechanochemical synthesis. The employed equipment used for the HEMM process was the Simoloyer CM01 apparatus from Zoz GmbH Co., Germany. The interior wall of the reaction chamber was coated by chemically stable silicon nitride, and the internal volume was 500 mL. The total amount of SiO and aluminum (50 g) was placed into the reaction chamber and ZrO_2 balls 5 μm in diameter were loaded at a ball-to-powder ratio of 20:1. The evacuation and purging of argon gas in the reaction chamber was repeated to build up and maintain an inert atmosphere inside the chamber. The rotational speed of grinding was 500 rpm, and several samplings were carried out during the grinding to characterize and evaluate the materials during a total reaction time of 50 h.

Characterization of Materials and Electrode. The crystalline structure analysis of the synthesized materials was performed using a Philips X'pert Pro X-ray diffractometer that was equipped with a Cu Kα source at 40 kV and 30 mA. The morphology, nanoscaled structure, and compositional analysis of the synthesized materials were examined using high-resolution transmission electron microscopy (HRTEM) (Model FEI F20, operating at 200 kV) and an energy-dispersive spectroscopy (EDS) system that was attached to the HRTEM system. Solid-state ^{29}Si MAS NMR and ^{27}Al MAS NMR analyses were performed at room temperature on a Bruker Advance III spectrometer with the resonance frequency of protons 400 MHz. Four millimeter (4-mm) zirconia ceramics rotors were used. The ^{29}Si MAS NMR data were collected at 79.49676 MHz, and the spinning frequency was 5500 Hz. A total of 256 scans were made within an excitation pulse length of 2.3 μs and a relaxation delay time of 1000 s. The ^{27}Al MAS NMR data were also collected at 104.43839 MHz, and the spinning frequency was 12 kHz. A total of 1024 scans were made using an excitation pulse length of 1 μs and a relaxation delay time of 10 s. Ex situ Fourier transform infrared (FT-IR) analysis of the lithiated $SiAl_{0.2}O$ and SiO electrodes were conducted with absorbance measurements in a Nicolet NEXUX 870 spectrometer with the spectral resolution of 4 cm^{-1} in the vibration frequency range from 400 cm^{-1} to 4000 cm^{-1}. After the cells reached the end of discharge, they were carefully disassembled and electrodes were subsequently rinsed with dimethyl carbonate (DMC), to remove residual electrolytes. They were then dried under vacuum for 3 h and pelletized after scraping out some powders from the dried electrodes and mixing them with KBr. The aforementioned procedures for FT-IR analysis were carried out in the dry room, providing humidity at a dew point of less than −40 °C. The morphology change of electrodes after cycling was analyzed by SEM (JEOL Model JSM-6700F). Similar to the ex situ FT-IR analysis, the cells were carefully disassembled and the electrodes were subsequently rinsed with DMC. They were then dried under vacuum for 3 h and transferred to the chamber of SEM equipment.

Electrode Fabrication and Electrochemical Test. Working electrodes were prepared by mixing 80 wt % active material ($SiAl_{0.2}O$ or SiO), 10 wt % carbon black (Super-P) as a conducting agent, and 10 wt % polyamidimide (PAI) resin as a binder, dissolved in *N*-methylpyrrolidinone (NMP) to form a slurry, followed by coating on a copper foil and drying at 200 °C for 1 h under vacuum. A coin cell assembly was prepared in standard 2016 coin cell hardware. A 1.3-cm-diameter disk of the working electrode was punched out from the $SiAl_{0.2}O$ or SiO anode laminate for use in the coin cell assembly. A lithium metal was used as a counter electrode. The counter electrode is 1.5-cm-diameter disks, which is larger than the working electrode. The working electrode was fixed in the center of the outer shell of the coin cell assembly using a spot welder and two drops of an electrolyte solution were added to fill the electrode. A 1 M $LiPF_6$ in a mixed solvent of ethylene carbonate (EC), diethylene carbonate (DEC), and ethyl methyl carbonate (EMC) (EC/DEC/EMC = 3/5/2 ratio) with a 10 wt % fluoroethylene carbonate (FEC) additive was used as an electrolyte solution. A 1.8-cm-diameter

(31) Gaskell, D. R. In *Introduction to the Thermodynamics of Materials*, 4th Ed.; Taylor & Francis: New York and London, 2003; Chapter 12.
(32) Ashby, M. F.; Jones, D. R. H. In *Engineering Materials 2: An Introduction to Microstructures, Processing and Design*, 3rd ed.; Butterworth−Heinemann Elsevier: Oxford, U.K., 2006; Chapter 15.
(33) Muchtar, A.; Lim, L. C. *Acta Mater.* **1998**, *46*, 1683.
(34) Lee, H. Y.; Lee, S. M. *Electrochem. Commun.* **2004**, *6*, 465.
(35) Ning, L. J.; Wu, Y. P.; Fang, S. B.; Rahm, E.; Holze, R. *J. Power Sources* **2004**, *133*, 229.

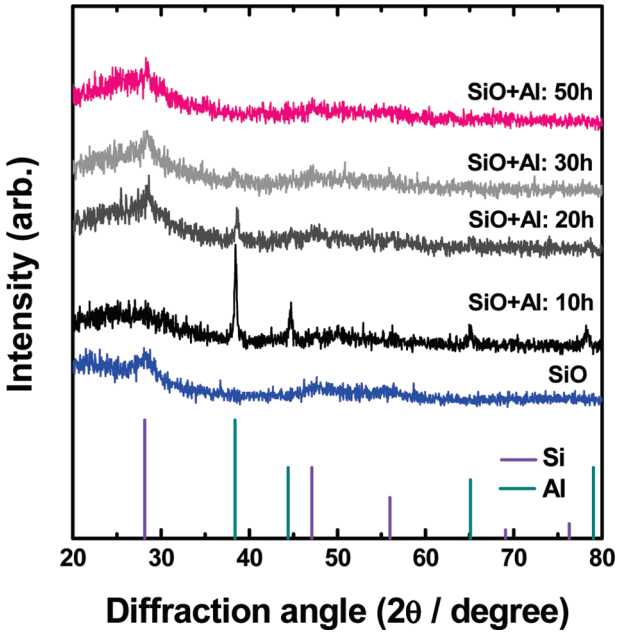

Figure 1. XRD patterns of SiO and $SiAl_{0.2}O$ at various reaction times of mechanochemical synthesis.

Celgard 2400 porous polyethylene separator was placed on top of the working electrode. A few drops of the electrolyte solution were added to the separator. The counter electrode was placed on the top of the separator, and special care was taken to align the counter electrode symmetrically above the working electrode. A stainless steel spacer and a Belleville spring were placed on top of the counter electrode. The above-positioned parts for assembly were crimped closed with a custom-build pneumatic crimping machine, using argon gas. The entire cell fabrication procedure was done in an argon-filled glovebox with < 1 ppm of both oxygen and moisture. The assembled cells were aged overnight at room temperature and then electrochemically tested using a TOSCAT 3000 U battery measurement system under the following protocols. The first cycle was operated at constant current (CC) mode of 60 mA/g within the voltage window of 0.005−2 V. The second cycle was also conducted galvanostatically but at a current density of 120 mA/g. The protocol of cycling test was constant current, followed by constant voltage (CCCV) mode for discharging (Li-insertion), in which 500 mA/g for the CC step and 0.005 V finished at 120 mA/g for the CV step, and CC mode for charging (Li-extraction) by 1.0 V. The cell impedance was recorded after every cycle with an AC impedance analyzer at a constant frequency (1 kHz) that was equipped for the TOSCAT 3000 U battery measurement system.

Results and Discussion

Structural and Chemical Characterization. To investigate the phase evolution of $SiAl_{0.2}O$ during mechanochemical synthesis, XRD analysis was performed and the results are shown in Figure 1. SiO, which is one of starting materials, exhibited weak diffraction patterns of silicon phases and a broadly weak background over the range of 20°−30°, which is attributed to an amorphous SiO_2 phase.[36] During the mechanochemical reaction between the SiO and Al, the diffraction pattern of the aluminum metal decreased gradually as the reaction time increased and totally disappeared after 50 h. The weak diffraction pattern, corresponding to the silicon phase in the SiO, became hard to find after 10 h, but started to reappear after 20 h and maintained its intensity and full width at half-maximum (fwhm) values up to 50 h. Based on the above results and the thermodynamic consideration mentioned previously, it is presumed that the main oxide phase of SiO_2 in the SiO partially reacted with the aluminum and was reduced to silicon nanocrystallites, accompanied by the formation of Al_2O_3. The expected Al_2O_3 is considered to be amorphous, since no related diffraction patterns could be found.

To clarify the compositional structure of matrix and the additional formation of silicon nanophases, we carried out solid-state ^{29}Si MAS NMR and ^{27}Al MAS NMR analyses for the $SiAl_{0.2}O$ material. A solid-state NMR technique is a well-known powerful analysis that can be used to enable us to identify chemical structures of disproportionated SiO[22] and amorphous aluminosilica materials.[37−41] Figure 2a shows the ^{29}Si MAS NMR spectra of the $SiAl_{0.2}O$ and SiO with relevant reference materials, e.g., Si and SiO_2. In the case of the SiO, three types of atomic neighborhoods were distinguished by their peaks from different chemical shifts. The higher shift peak at −110 ppm, relative to a tetramethyl silane (TMS) standard, was related to Si(O4) tetrahedra in SiO_2 regions. The lower broad peak around −69 ppm exhibited fractions from elemental amorphous silicon or its suboxides, and a little sharp peak at −81 ppm corresponds to crystalline silicon.[22] For the mechanochemically synthesized $SiAl_{0.2}O$, similar spectral patterns were observed, except the peak around −101 ppm. The spectra around −69 ppm and the weak peak at −81 ppm were assigned to elemental silicon or suboxides similar to the SiO. As for the spectra from Si(O4) tetrahedra, however, a somewhat different resonance position located at the less-downfield shift of −101 ppm was observed. This different chemical shift was considered to have resulted from changes of the chemical environment around the Si^{4+} via Al^{3+} incorporation, which has been discussed well in many NMR studies for amorphous aluminosilica or aluminosilicate materials.[37−40] Generally, environmental conditions surrounding a Si atom in aluminosilica materials can be defined by $Q_m(n\mathrm{Al})$, where m (≤ 4) is the number of bridging oxygens and n ($\leq 4 - m$) is the number of Al atoms present as second-nearest neighbors.[38] The SiO_2 phase—namely, $Q_4(0\mathrm{Al})$—shows a chemical shift of Si^{4+} at −110 ppm, the aluminosilica of $Q_4(1\mathrm{Al})$ exhibits at −104.8 ppm, $Q_4(2\mathrm{Al})$ at −99.4 ppm, and $Q_4(3\mathrm{Al})$ at −94 ppm.[37] For the $SiAl_{0.2}O$, the chemical shift of Si^{4+} around −101 ppm was presumed to result from the neighboring

(36) Kapaklis, V. *J. Non-Cryst. Solids* **2008**, *354*, 612.
(37) Criado, M.; Fernandez-Jimenez, A.; Palomo, A.; Sobrados, I.; Sanz, J. *Microporous Mesoporous Mater.* **2008**, *109*, 525.
(38) Engelhardt, G.; Noftz, M.; Forkel, K.; Wishmann, F. G.; Magi, M.; Samson, A. *Phys. Chem. Glasses* **1985**, *26*, 157.
(39) Matsuya, S.; Maeda, T.; Ohta, M. *J. Dent. Res.* **1996**, *75*, 1920.
(40) Hensen, E. J. M.; Poduval, D. G.; Magusin, P. C. M. M.; Coumans, A. E.; van Veen, J. A. R. *J. Catal.* **2010**, *269*, 201.
(41) May, M.; Asomoza, M.; Lopez, T.; Gomez, R. *Chem. Mater.* **1997**, *9*, 2395.

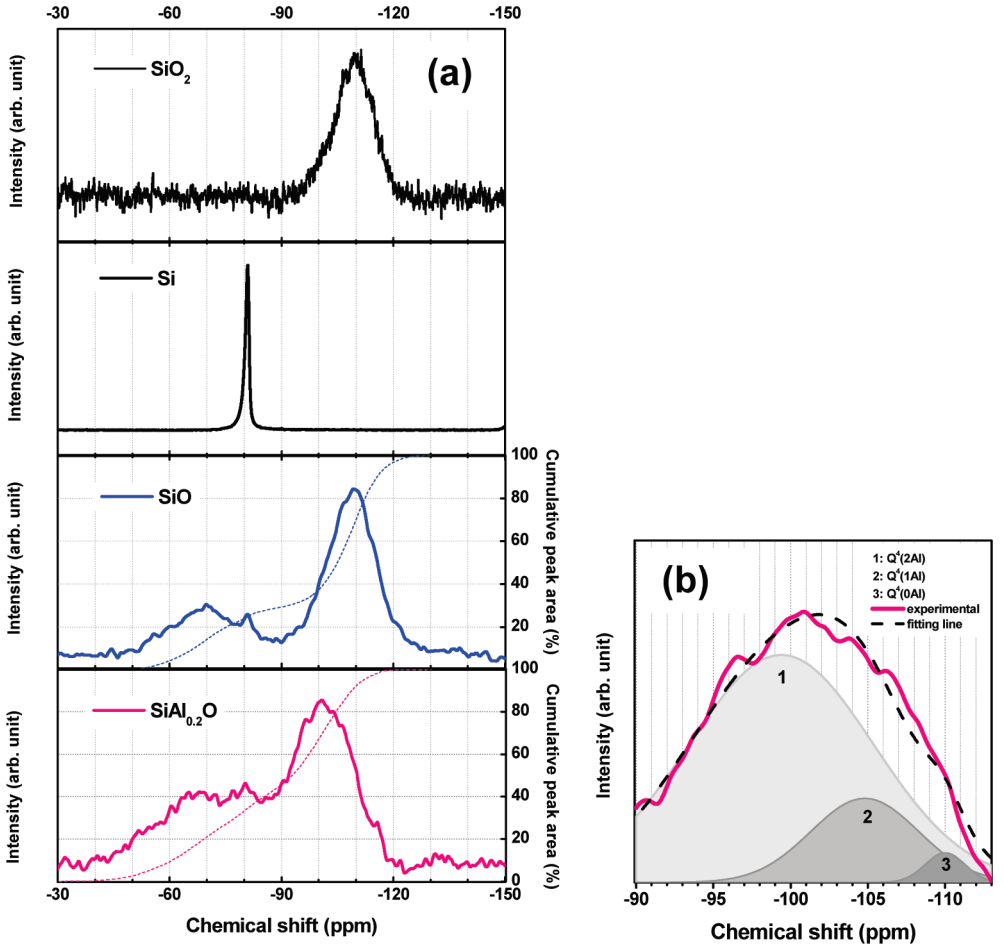

Figure 2. (a) ^{29}Si MAS NMR spectra of $SiAl_{0.2}O$, SiO, Si, and SiO_2; the integral intensity also is plotted, in the case of $SiAl_{0.2}O$ and SiO. (b) Decomposition of the ^{29}Si MAS NMR spectra around −101 ppm of $SiAl_{0.2}O$ with Q_4(2Al), Q_4(1Al), and Q_4(0Al).

of more than one Al^{3+} and decomposed for a quantitative understanding with several $Q_m(n\text{Al})$ peaks, which were assumed as Gaussian profiles.[39] Using the decomposition results as shown in Figure 2b, the occupation ratio of Q_4(0A1)—namely, the SiO_2 phase in the $SiAl_{0.2}O$—was only ca. 2.2%. Instead, the new contributions of Q_4(1Al) and Q_4(2Al) were estimated and their occupation ratios were 17.4% and 80.4%, respectively. This means that the unreacted SiO_2 phase in the SiO during the mechanochemical synthesis was restructured with the expected Al_2O_3 and, consequently, new aluminosilica matrix phases were estimated, in which most of the Si^{4+} were neighbored with two Al^{3+} over oxygens.

In the ^{27}Al MAS NMR results presented in Figure 3, the $SiAl_{0.2}O$ exhibited very intricate spectra, having three peaks at ca. 45, 21, and −3 ppm, while Al_2O_3, as a reference material, showed two main peaks, at 0 and 60 ppm. There have been many reports about ^{27}Al MAS NMR studies for various structures of an alumina component in aluminosilicas or aluminosilicates,[40,41] and it can be summarized that the chemical shift of tetrahedral alumina Al(O4) appears between 50 and 70 ppm, the pentacoordinated alumina Al(O5) at around 25−30 ppm, and the octahedral alumina Al(O6) at around 0−11 ppm. Based on these reports, the Al_2O_3 of a reference sample in our study was identified to have two types of tetrahedral

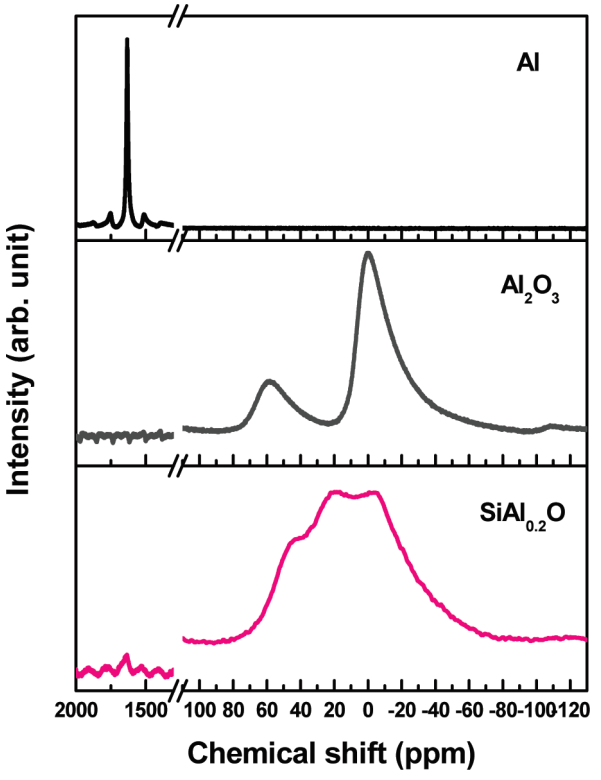

Figure 3. ^{27}Al MAS NMR spectra of $SiAl_{0.2}O$, Al_2O_3, and aluminum.

and octahedral structures and the $SiAl_{0.2}O$ was recognized to have the pentacoordinated alumina structure, in addition to the tetrahedral and octahedral structures. According to ref 41, the formation of pentacoordinated alumna Al(O5) is closely related to the existence of structural defects and nonstoichiometric structures reducing the network connectivity of aluminosilicates. In mechanochemical synthesis, the temperature can rise above 300 °C and the pressures to which the ingredients are subjected can reach up to 6 GPa, so its products commonly contain internal stresses and a high density of lattice defects.[42] These circumstances are considered to bring about the formation of the pentacoordinated alumina Al(O5), accompanied by structural defects or voids in the mechanochemically synthesized $SiAl_{0.2}O$. Although a weak signal corresponding to metallic aluminum at 1630 ppm[43] was found, its relative integral intensity was 3% and negligible, compared to the total alumina intensity of 97%. This means that aluminum metal as a starting material was almost oxidized and converted to alumina after the mechanochemical reaction with SiO.

More information from the NMR analyses involves relative estimations for the additional formation of new silicon nanophases by the mechanochemical reaction between SiO and aluminum. In the case of the SiO, the relative integral intensities of the peaks corresponding to Si and SiO_2 were 30% and 70%, respectively (see Figure 2a). According to Hohl et al.,[22] the atomic nuclei located near unpaired electrons do not contribute to the peaks in the NMR spectrum, which is the so-called "wipe-out effect". By this effect, the deficiency in the signal of the silicon phase is fairly noticeable while the signal of SiO_2 and suboxide peak is almost unaffected. That is a reason for the differently estimated quantitative ratio, compared to the expected half-and-half ratio between Si and SiO_2 in the disproportionated SiO. For the $SiAl_{0.2}O$, the relative integral intensities of the peaks corresponding to Si and SiO_2 were 42% and 58%, respectively (see Figure 2a). In comparison with the SiO, the relative increase of integral intensity corresponding to silicon nanophases in the $SiAl_{0.2}O$ was identified and, therefore, we could verify the new formation of silicon nanophases after mechanochemical reaction between SiO and aluminum, in addition to the formation of several aluminosilica structures.

Based on the results achieved so far from the NMR and XRD analyses, the reaction chemistry of the $SiAl_{0.2}O$ formation was organized as follows:

$$\begin{aligned} &SiO + 0.2Al = 0.5Si + 0.5SiO_2 + 0.2Al \\ &\rightarrow 0.5Si\ (\text{originally existing}) + 0.15Si\ (\text{newly generated}) \\ &+ 0.35SiO_2 + 0.1Al_2O_3 \rightarrow 0.65Si \\ &+ Si_{0.35}Al_{0.2}O\ (\text{aluminosilica}, 0.35SiO_2 \cdot 0.1Al_2O_3) \quad (5) \end{aligned}$$

The apparent stoichiometries of the aluminosilica in the $SiAl_{0.2}O$ also could be estimated experimentally from the decomposition results of the ^{29}Si MAS NMR spectra. When the apparent chemical formula of the $Q_4(2Al)$ unit is represented as $Si_3Al_2O_9$, the $Q_4(1Al)$ unit as $Si_4AlO_{9.5}$, and the $Q_4(0Al)$ unit as Si_5O_{10}, the final molar ratio among Si, Al, and O calculated from the occupation ratio of the previous decomposed $Q_m(n\text{Al})$ data was $Si_{0.353}Al_{0.196}O$. This stoichiometry is almost as same as that derived with respect to the thermodynamics, as per eq 5.

Figure 4 exhibits the results of TEM analysis for the $SiAl_{0.2}O$, indicating its nanoscaled structural characteristics. Uniform distributions of Si, Al, and O all over a particle were identified from TEM-EDS elemental mapping analysis. The distinctive composite structure of island-typed crystallites embedded in an amorphous matrix was also verified from HRTEM images and selected-area electron diffraction (SAED) patterns. The crystallites showed sizes of 5−10 nm and were confirmed as silicon phases, assigned an Si(111) *d*-spacing value of 0.3 nm. In summary, the mechanochemically synthesized $SiAl_{0.2}O$ was not a single-phase material and still maintained the island−matrix nanocomposite structure as equally found in SiO. More specifically, it had island-type silicon nanocrystallites embedded in an amorphous matrix phase composed of Si, Al, and O. Based on the ^{29}Si MAS NMR and ^{27}Al MAS NMR results, the amount of dispersed silicon nanocrystallites was larger than the amount of SiO and the compositional structure of the matrix was regarded as aluminosilica with a composition of $Si_{0.35}Al_{0.2}O$ ($= 0.35SiO_2 \cdot 0.1Al_2O_3$), as illustrated schematically in Figure 4c.

Electrochemical Performance of $SiAl_{0.2}O$. Figure 5 shows the first discharge (Li insertion) and charge (Li extraction) voltage profiles of $SiAl_{0.2}O$, compared with SiO. The discharge capacity of the $SiAl_{0.2}O$ was ca. 2240 mAh/g, which was smaller than that of the SiO (2400 mAh/g). The electrochemical reaction mechanism of SiO at the first cycle is still not precise and is controversial, but it has been generally considered that the discharge products of SiO are Li_4SiO_4 or Li_2O, as electrochemically irreversible phases, and $Li_{3.75}Si$, as a reversible phase.[16,17,21,28] The smaller discharge capacity in the $SiAl_{0.2}O$ was considered to have originated from the lithium-inactive alumina component in the aluminosilica matrix of $SiAl_{0.2}O$ and it could be verified by FT-IR analysis for discharged $SiAl_{0.2}O$ electrodes as follows. First of all, we performed FT-IR analysis on the $SiAl_{0.2}O$ and the SiO in their initial states; the results are presented in Figure 6a. The absorption bands related to the alumina component in the $SiAl_{0.2}O$ could not be found, and it is believed that they are relatively weak and veiled by the strong absorption bands of Si(O4) tetrahedra, appearing at ~1020, 800, and 460 cm^{-1}.[24,44] The strong broad band at ~1100 cm^{-1} of the Si(O4) tetrahedra in SiO, however, shifted to a higher wavelength region, i.e., toward 1000 cm^{-1}, after the formation of the $SiAl_{0.2}O$. It indicates that substitution of the alumina occurred into the silica structure[45] and can represent more indirect evidence for the alumina component in

(42) Suryanarayana, C. *Prog. Mater. Sci.* **2001**, *46*, 1.
(43) Sun, B. A.; Pan, M. X.; Zhao, D. Q.; Wang, W. H.; Xi, X. K.; Sandor, M. T.; Wu, Y. *Scr. Mater.* **2008**, *59*, 1159.
(44) Tsu, D. V.; Lucovsky, G.; Davidson, B. N. *Phys. Rev. B* **1989**, *40*, 1795.
(45) Xia, L.; Wen, G.; Song, L.; Wang, X. *Mater. Chem. Phys.* **2010**, *119*, 495.

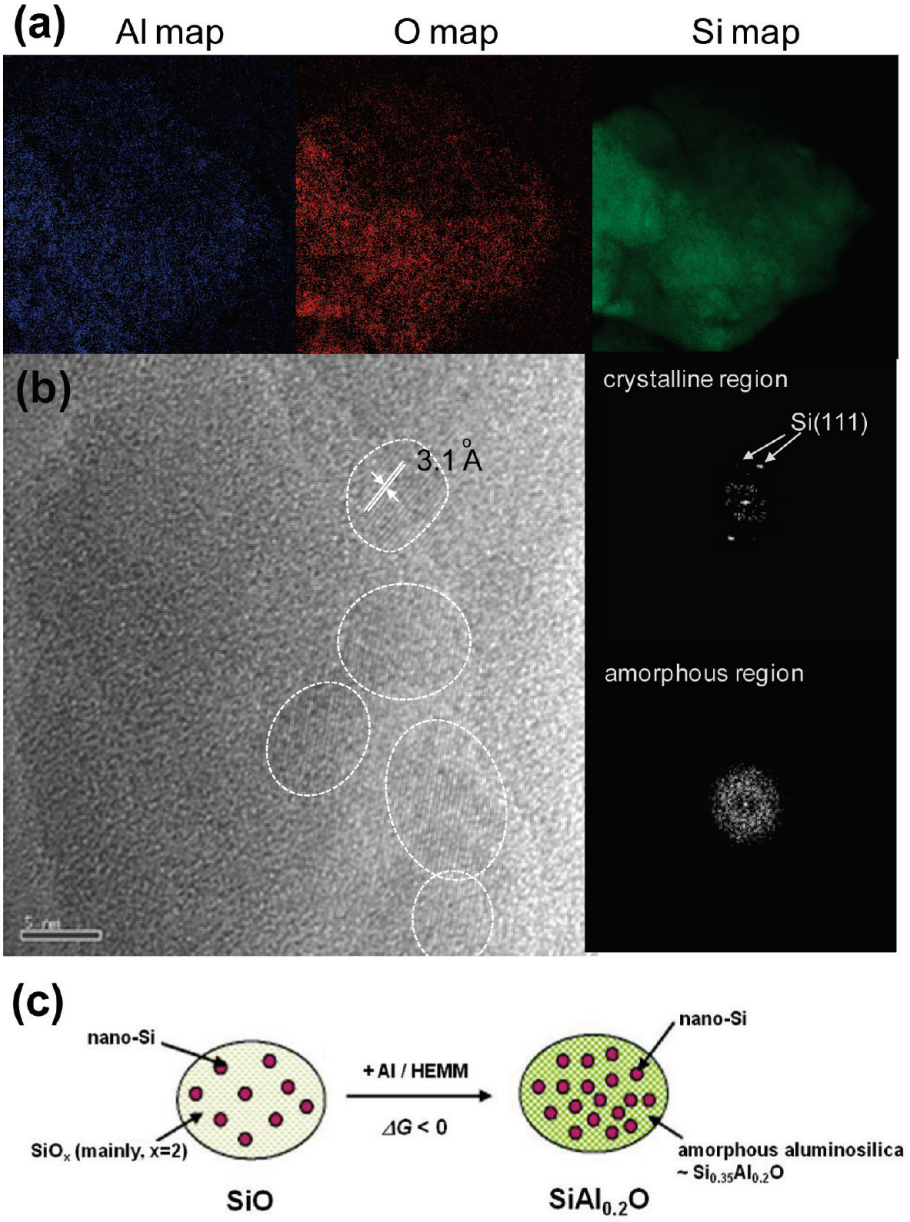

Figure 4. (a) TEM-EDS elemental mapping of a $SiAl_{0.2}O$ particle; (b) HRTEM image and corresponding SAED patterns indexed with lattice spacing; and (c) schematic illustration of nanostructured $SiAl_{0.2}O$ material.

the $SiAl_{0.2}O$. Figure 6b shows the FT-IR spectra of the lithiated $SiAl_{0.2}O$ and SiO electrodes after the first discharge. As for the SiO electrode, all characteristic spectra of the SiO_2 phase disappeared and a minor absorbance band was found, except for the weak spectra at 500 cm^{-1}. The disappearance of the spectra corresponding to SiO_2 reflects the electrochemical reactivity of SiO_2 phase in disproportionated SiO with lithium, and the observed spectra at 500 cm^{-1} is considered to be from the formation of Li_2O.[46] As for the $SiAl_{0.2}O$ electrode, all characteristic spectra of the silica component in the aluminosilica matrix disappeared in the same way as the SiO, but distinguishable absorption bands in the region of 1000−700 cm^{-1} were observed. According to several FT-IR studies about alumina structures, the characteristic absorption bands of Al(O6) octahedra appear in the region of 800−950 cm^{-1} (ref 47) and Al(O4) tetrahedra in the region of 720−780 cm^{-1} and around 550 cm^{-1}.[48,49] Based on these reports, the observed absorption bands in the region of 1000−700 cm^{-1} in the $SiAl_{0.2}O$ electrode could be assigned to alumina, more specifically, of Al(O6) octahedra rather than Al(O4) tetrahedra. This is consistent with the ^{27}Al MAS NMR results showing pentacoordinated and octacoordinated aluminas as the main structures, reflecting the relatively low homogeneous mixing of alumina with silica by defects or voids in its structure.[41,50] From the above FT-IR analyses, it was verified that the silica component of the aluminosilica in $SiAl_{0.2}O$ was also electrochemically reactive with lithium

(46) Osaka, T.; Shindo, I. *Solid State Commun.* **1984**, *51*, 421.
(47) Roy, B. N. *J. Am. Ceram. Soc.* **1987**, *70*, 183.
(48) Lin, M. H.; Wang, M. C. *J. Mater. Sci.* **1995**, *30*, 2716.
(49) Ghosh, N. N.; Pramanik, P. *Br. Ceram. Trans.* **1997**, *96*, 155.
(50) Selvaraj, U.; Komarneni, S.; Roy, R. *J. Am. Ceram. Soc.* **1990**, *73*, 3663.

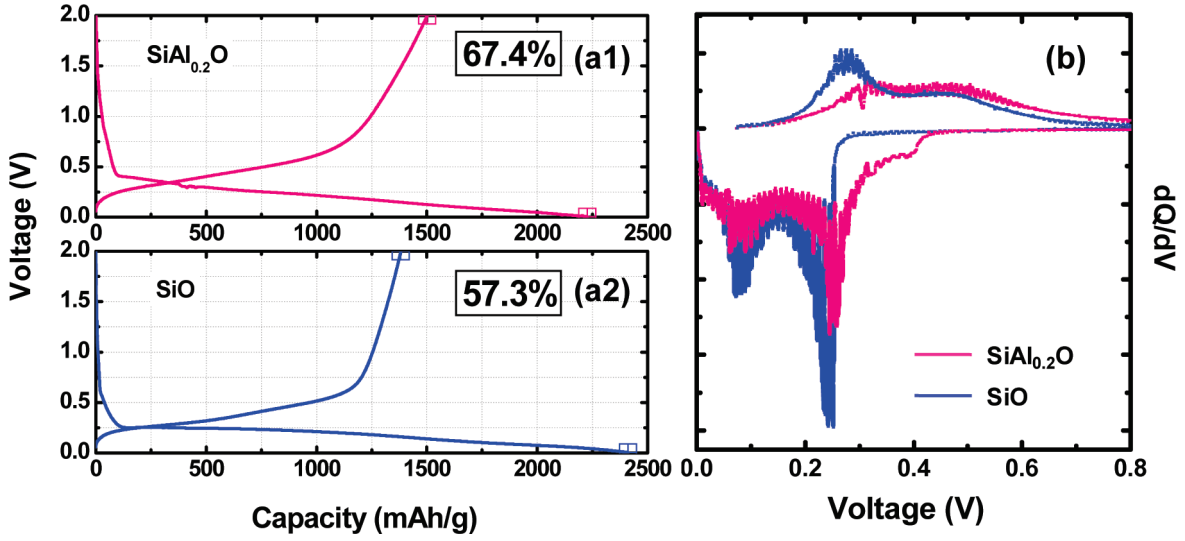

Figure 5. (a) Voltage profiles and (b) differential capacity plots of $SiAl_{0.2}O$ and SiO electrodes at the first cycle. Numbers shown inside the voltage profile plot indicate its initial Coulombic efficiency (ICE).

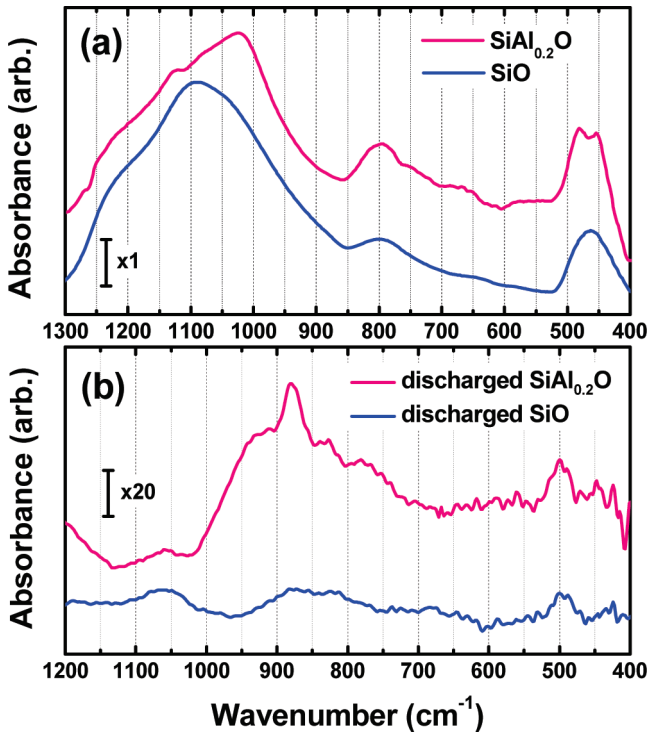

Figure 6. FT-IR spectra of (a) $SiAl_{0.2}O$ and SiO and (b) $SiAl_{0.2}O$ and SiO electrodes after the first discharge.

and presumed to follow the same reaction mechanism as that for the SiO, with respect to the identical peak appearance at 500 cm^{-1}, caused by Li_2O formation. More importantly, the alumina in the aluminosilica was verified to be electrochemically inactive with lithium and still remained in the discharged $SiAl_{0.2}O$. The remained alumina phase was a reason for the decreased discharge capacity of $SiAl_{0.2}O$, compared to SiO, and its expected important role in cycling performance of $SiAl_{0.2}O$ is to be discussed later.

One of the improved performances of the $SiAl_{0.2}O$ as an anode material was the increased initial Coulombic efficiency (ICE), compared to SiO. One major demerit of SiO in practical application to lithium batteries is its low ICE, which generally results from the initial irreversible reactions and its low intrinsic electrical conductivity.[17−21] The ICE of SiO can be improved by enhancing its electrical conductivity via carbon coating on SiO[19,30] or intimate carbon composite.[15,18] In our study, however, we tried to understand the chemistry of phase transitions related to ICE, under the condition of their own intrinsic properties, and evaluated electrochemical performances of $SiAl_{0.2}O$ or SiO without any electrical modifications. Under our experimental conditions, the SiO showed an ICE value of 57.3%, but the $SiAl_{0.2}O$ exhibited a relatively increased ICE value of 67.4% (see Figure 5a). Considering that the SiO_2 phase in disproportionated SiO is electrochemically reactive and acts as a source of the initial irreversible reaction, the partial conversion of the SiO_2 phase into both the lithium-inactive alumina and the silicon nanophase as reversible reaction sites in $SiAl_{0.2}O$ resulted in the increased ICE.

Figures 7a and 7b show the cycling performance of $SiAl_{0.2}O$, compared with SiO. The $SiAl_{0.2}O$ exhibited a slight decrease in capacity during the early cycles but maintained a reversible capacity of 800 mAh/g until 100th cycle, while the SiO showed a steady decrease in capacity with cycling. The reversible efficiency at every cycle in the $SiAl_{0.2}O$ was also higher than that for the SiO, which is $>99.5\%$ at steady state (see Figure 7c). The enhanced cycling performance of $SiAl_{0.2}O$ was also understood by measuring the cell impedance during cycling. In lithium-alloy anode systems, not only the pulverization of active materials but also the repeated volume changes of electrodes itself also causes a gradual collapse of the electrical network among components, i.e., active materials and conducting agents with binder inside composite electrodes. They result in an increase in the impedance in electrodes and, finally, a decrease in capacity with cycling. Figure 7d shows the variation of the cell impedance during cycling, measured by an AC impedance analyzer at a constant frequency of 1 kHz after every end of charge

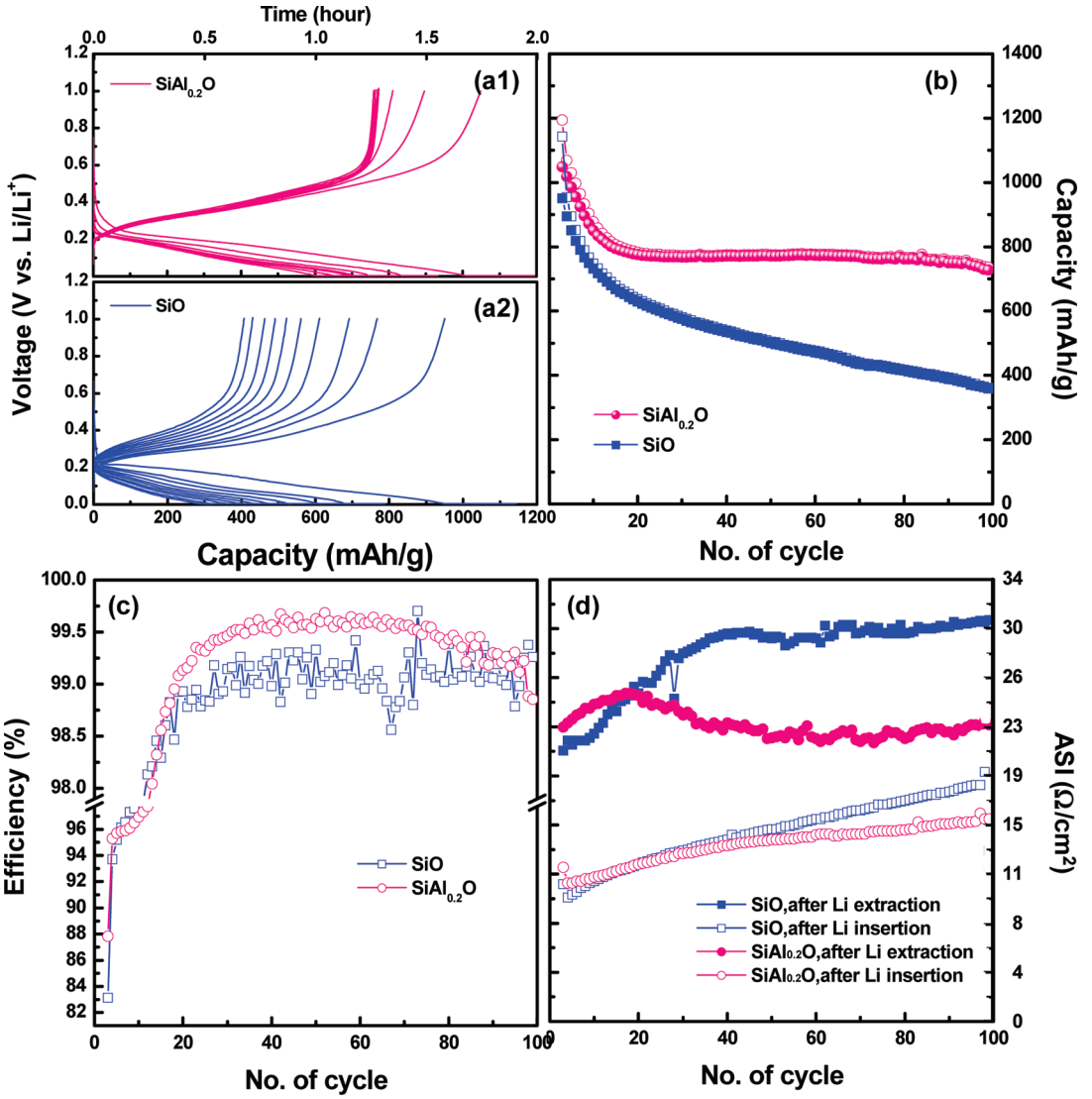

Figure 7. Cycling performance of $SiAl_{0.2}O$, compared to SiO: (a) voltage profiles of charge and discharge, (b) capacity retention of Li extraction, (c) reversible efficiency, and (d) variation of cell impedance with cycling.

and discharge. In both cells, the impedance measured after charge (Li extraction) was higher than that measured after discharge (Li insertion). Normally, the mechanical fractures in active materials and the loosened network of composite electrodes can be observed well after the contraction of active materials (that is to say, the charged state rather than expansion).[51] These behaviors were considered to bring about less electrical contact points inside electrodes and therefore result in higher impedance after charge than discharge. In association with the behaviors of capacity retention during cycling, the cell impedance after charge rather than discharge seems to be more relevant for evaluating the cycling performance of anode materials. For the SiO, the impedance abruptly increased by the 30th cycle and showed its continuous increase until the 100th cycle. This behavior is very similar to the capacity retention during cycling, in which the capacity also is abruptly decreased by the ca. 30th cycle and continued its decrease until the 100th cycle. For the $SiAl_{0.2}O$, the gradual increase of impedance in the early stage was also observed. However, the impedance after the 20th cycle started to decrease inversely and was stabilized up to the 100th cycle. This behavior is also well-matched with the capacity retention of the $SiAl_{0.2}O$ during cycling. From the analogy of behaviors between the impedance after charge and the capacity retention in cycling, the critical impact of the electrical network in electrodes on cycling performance was confirmed and the cell impedance after charge could be accepted as another parameter for representing the cycling performances of silicon-based anode materials.

We have supposed that the improvement of cycling performance in $SiAl_{0.2}O$ is closely related to the mechanically more stabilized nanostructure of $SiAl_{0.2}O$, compared to SiO. As generally known, a main reason for degradation in cycling performance in a lithium-alloy anode system is the mechanical deterioration of active materials, such as cracking and fracturing by volume change when lithium is inserted and extracted. This induces an electrical contact loss of active materials and consequently results in capacity

(51) Beaulieu, L. Y.; Eberman, K. W.; Turner, R. L.; Krause, L. J.; Dahn, J. R. *Electrochem. Solid State Lett.* **2001**, *4*, A137.

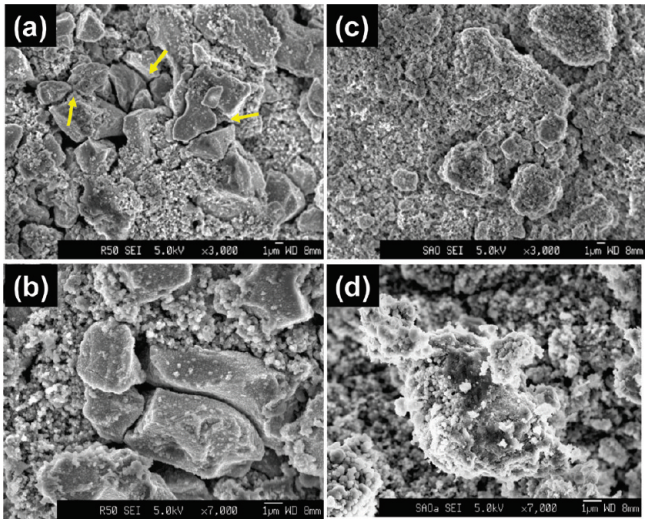

Figure 8. SEM images of (a,b) the SiO electrode and (c,d) the $SiAl_{0.2}O$ electrode after the 50th cycle.

loss during cycling. Figure 8 shows scanning electron microscopy (SEM) images of the $SiAl_{0.2}O$ and SiO electrodes after the 50th cycle. While severe cracking and fracture were found in the cycled SiO particles, little mechanical pulverization was observed in the $SiAl_{0.2}O$. We have believed that the suppression of fracture in the $SiAl_{0.2}O$ electrode is due to lithium-inactive alumina existing as a matrix component in the $SiAl_{0.2}O$, which enhances the mechanical stability of this nanostructured material.

Recently, many attempts to understand and resolve the pulverization phenomena of lithium-alloy anode materials, from a mechanics point of view, have been reported. Aifantis et al.[52] developed the design criteria for active/inactive nanocomposite anode materials based on theoretical fracture mechanics and suggested that higher fracture toughness and lower ultimate tensile strength of the matrix were preferable for allowing greater critical crack length prior to fracture. Chen et al.[53] investigated experimentally the behaviors of crack formation and propagation in Sn and Ni−Sn thin-film anodes having different ductility by nanoindentation and nanowear tests. Huggins et al.[54] presented a mechanistic explanation of the relationship among flaw critical size, phase transformation strains, and fracture toughness. Sohn et al.[55] suggested a novel composite design for anode materials, applying the principle of particulate-reinforced metal-matrix composites, which exhibit enhanced fracture toughness to achieve higher resistance to crack initiation and propagation. Alumina is a well-known engineering ceramic material that exhibits a high level of fracture toughness and has been used in many applications that require durable mechanical properties.[32] The fracture toughness of alumina[32,33] is in range of 4−6 MPa $m^{1/2}$; this value is higher than that of glassy lithium oxide and lithium silicates, which are considered as matrix phases in the discharged SiO, the fracture toughness of which is in the range of 0.6−1.1 MPa $m^{1/2}$.[56,57] Based on the aforementioned references[52−55] and the superior mechanical properties of alumina, it has been believed that employing alumina as a matrix component in active/inactive nanocomposite anode materials could enhance the mechanical stability against fracture that occurs via volume changes during charge and discharge reactions. Designed optimally, with respect to structure and quantity, alumina can be a preferred material as a matrix component in nanocomposite anode materials for lithium batteries.

Conclusions

In this study, we have developed and characterized a nanostructured $SiAl_{0.2}O$ composite material and investigated its electrochemical performance as an anode for lithium rechargeable batteries. Based on the results of various analytical techniques, the $SiAl_{0.2}O$ was not a single phase and maintained the island−matrix nanocomposite structure that also is found in SiO. More specifically, it was composed of silicon nanocrystallites, each of which was < 10 nm in size and their amount was relatively greater, compared to SiO, in an amorphous matrix consisting of Si, Al, and O. The compositional structure of the matrix was amorphous $SiO_2 \cdot Al_2O_3$, namely, aluminosilica in which most of Si atoms were neighbored with two Al atoms over oxygen. When evaluating the electrochemical performance of the $SiAl_{0.2}O$ electrode, remarkable improvements in both the increased initial Coulombic efficiency (ICE) and cycling performance could be obtained. It represented a relative increase of ca. 10% in ICE versus SiO and a reversible capacity of 800 mAh/g over 100 cycles. Little mechanical pulverization and less impedance change during cycling were also found and resulted in improved cycling performance. The new formation of both the lithium-inactive alumina and the additional silicon nanocrystallites in the $SiAl_{0.2}O$ enhanced the ICE by partially replacing SiO_2, which is regarded as an origin of the initial irreversible reaction, and the lithium-inactive alumina was also believed to play an important role in suppressing the mechanical deterioration of the $SiAl_{0.2}O$ when the silicon nanocrystallites react with lithium reversibly and repeatedly, accompanying volume changes of the particles. Magnesium, calcium, and titanium can be explored in the same way as aluminum to improve the ICE and cycling performance of SiO, and carbon coating or intimate carbon composite of the $SiAl_{0.2}O$ can be attempted to obtain the practically applicable ICE and better cycling performance for further works.

Acknowledgment. We thank to Prof. Ju Cheol Park at the Research Institute of Advanced Materials, Seoul National University, for the HRTEM analyses and discussions.

(52) Aifantis, K. E.; Hackney, S. A.; Dempsey, J. P. *J. Power Sources* **2007**, *165*, 874.
(53) Chen, J.; Bull, S. J.; Roy, S.; Kapoor, A.; Mukaibo, H.; Nara, H.; Momma, T.; Osaka, T.; Shacham-Diamand, Y. *Tribol. Int.* **2009**, *42*, 779.
(54) Huggins, R. A.; Nix, W. D. *Ionics* **2000**, *6*, 57.
(55) Jeong, G.; Kim, Y. U.; Sohn, H.-J.; Kang, T. *J. Power Sources* **2001**, *101*, 201.
(56) Bar, K.; Chu, C. Y.; Singh, J. P.; Goretta, K. C.; Routbort, J. L.; Billone, M. C; Poeppel, R. B. *Fusion. Eng. Des.* **1989**, *8*, 371.
(57) Sehgal, J.; Ito, S. *J. Non-Cryst. Solids* **1999**, *253*, 126.